Prestack Seismic Data Inversion for Shale Gas Reservoir Characterization in China*

Gang Yu[1], Yusheng Zhang[1], Uwe Strecker[2], and Maggie Smith[2]

Search and Discovery Article #41829 (2016)**
Posted July 25, 2016

*Adapted from extended abstract prepared in relation to oral presentation at GEO 2016, 12th Middle East Geosciences Conference and Exhibition, Manama, Bahrain, March 7-10, 2016. Bahrain:

[1]BGP Inc. (yugang03@cnpc.com.cn)
[2]Rock Solid Images INC

Abstract

An integrated study of the well Zhao-104 and surrounding wide-azimuth 3D seismic volume within the shale gas reservoir in South China has been conducted with the objective of generating shale formation properties related to fracture orientation and intensity in the area and deriving such reservoir rock properties as data quality allows.

The inversion for P and S impedance and derivative attributes produced volumes that relate to rock properties, such as brittleness and rigidity, that are likely to impact fracturing. Seismic attribute analysis of anisotropy from elliptical velocity inversion indicates that anisotropy varies horizontally and vertically and that it is dominantly controlled by stress azimuth, which conforms to the current day stress field as independently determined from borehole break-outs.

Introduction

An integrated study of the well Zhao-104 and surrounding wide-azimuth 3D seismic data volume within the shale gas reservoir in South China has been conducted with the objective of generating shale formation properties related to fracture orientation and intensity in the area and deriving such reservoir rock properties as data quality allows. Well data, structural seismic information and prestack inversion products were combined in an integrated interpretation.

Seismic gather conditioning improved seismic data quality prior to prestack inversion by improving signal/noise ratio, removing NMO stretch and aligning reflection events. Velocities from residual moveout (RMO) analysis on individual sectors were used as input to detection of fracture orientation and anisotropy.

Fracture strike and P wave anisotropy were calculated using the RMO updated sector velocity fields in elliptical velocity inversion, while inversion for P and S impedance and derivative attributes produced volumes that relate to rock properties, such as brittleness and rigidity that are likely to impact fracturing.

Inversion of Seismic Data

During the prestack inversion process, the velocity field was updated after residual moveout analysis for each sector and used in elliptical velocity inversion to determine degree and direction of anisotropy.

A simultaneous inversion for P and S impedance using the angle stacks was performed for each sector, but the results were judged insufficiently stable to proceed to inversion for Thomsen parameters and elastic moduli (Thomsen, 1986). Instead an isotropic inversion of full azimuth angle stacks was performed, the higher fold giving rise to a more stable inversion. Additional attributes, such as Dynamic Young's Modulus * Density (ERho), which is proportional to brittleness, and Mu Rho, an indicator of rigidity, were calculated.

Elliptical Velocity Inversion

In a system of Horizontal Transverse Isotropy (HTI) the model is parallel vertical cracks (Thomsen, 1988). P waves travel with different velocities depending on their travel path with respect to the fracture system, fastest direction being parallel to fracture orientation, slowest perpendicular (Thomsen, 1995). Wide azimuth 3D seismic data is divided into azimuthal sectors and independent velocity analyses run on each. An ellipse is fitted to the sector velocity values and V_{Pfast} and V_{Pslow} calculated. The major axis or V_{Pfast} direction is parallel to fracture strike and the degree of anisotropy is given by P wave Anisotropy = $(V_{Pfast} - V_{Pslow})/ V_{Pfast}$. Figure 1 shows the concept of *azimuth of anisotropy*.

Residual moveout analysis was run on each of the azimuthally sectored data sets and corrections applied to the RMS velocity field, creating four updated sector velocity volumes which were smoothed and input to elliptical velocity inversion. In Figure 2 vectors representing the direction and intensity of anisotropy are overlays on a coherency extraction. There is good correspondence between areas of highest coherence (lightest colors) and lowest values of anisotropy.

Simultaneous Inversion

Simultaneous inversion finds a global solution for model P and S impedances that best fits the input data. Input data consists of seismic angle stacks connected to well information through well-tie and wavelet extraction. Well data is also used in the low frequency model along with interpreted horizons for structural control. The seismic velocity field provides low frequency impedance trends away from the well. Figure 3 is the inversion workflow.

Primary outputs are P and S impedance. Calculation of density requires better data quality and wider angle range than was present in this data set. Impedance attributes can then be combined to produce attributes directly relatable to reservoir properties, for example, Poisson's ratio.

Well Tie

The synthetic to seismic tie was reasonable at the zone of interest for all sectors. However, the quality tends to deteriorate in the shallower section. Also of some concerns are the weak near and far offsets seen on the seismic data compared to the synthetic. The panel for sector 2 is displayed in Figure 4. Note also that each angle stack has poor event continuity and high noise content above the zone of interest.

Wavelet Extraction

Wavelets link the amplitude and frequency of each angle stack to reflectivity. Wavelets may be extracted in a number of ways, often by convolving with the log-based reflectivity series. The convolutional method requires a window length ideally 500 ms or larger. Here, that means including several hundred milliseconds above the zone of interest where section is very noisy on all angle stacks and the tie to the synthetic is poor. The resulting wavelets were unstable. An alternative method estimates statistical zero phase wavelets that match seismic amplitude spectra, allowing a larger spatial window to be used for improved signal to noise ratio. Phase information is not captured; however, the seismic volume is thought to be close to zero phase. Wavelets for sector 3 are shown in Figure 5. The cross correlations have their maximum at zero lag and roughly symmetrical side lobes, confirming the zero phase assumption. Note that the symmetry tends to decrease with increasing angle and the correlation coefficient drops, both indicative of increased noise in the data.

Low Frequency Model

The low frequency model bridges the low frequency gap between well data; it has frequencies from zero to kilo-Hertz and band-limited seismic data that often has a low cut of around 6-8 Hz and also serves as the *a priori* geological model in the simultaneous inversion. Well control is often sparse, in this case a single well, and so the seismic velocity field was used as a modulating influence away from the well location. The workflow (Figure 6) incorporated well data, structural information in the form of interpreted TS horizon, copied and time-shifted to bound the inversion window and the seismic velocity field as follows:

- Upscale well logs to 8 Hz and extrapolate in a structural framework built from horizons producing 100% well based model;
- Calculate an interval velocity cube from smoothed seismic RMS velocities and calibrated to upscaled log having similar frequency (~2 Hz);
- Extrapolate calibration factor in horizon framework and apply calibration factor to seismic interval velocities;
- Apply transforms from upscaled well logs to obtain seismic based V_S and density, and combine with interval velocity to produce seismic-based impedances;
- The 100% well trends may then be combined with the calibrated seismic in varying proportions depending on the confidence in the various sources of information. In this case 65% well and 35% calibrated seismic (Figure 7).

Inversion QC

Inversion results were evaluated by comparing traces extracted from the seismic inversion to corresponding log data upscaled to seismic

frequencies. Additionally synthetic angle stacks, products of the inversion, can be compared to the input angle stacks and the difference between the two, commonly called "residuals" is also inspected.

In Figure 8 attributes extracted from seismic volumes are compared to log data. The *P* impedance result compares favorably with log data; however, the *S* impedance is a poorer match. This situation often arises when data quality is unreliable. Nevertheless, the resulting Poisson's ratio, while somewhat overdriven, has the correct sense.

Input angle stacks and the synthetic results from inversion in Figure 9 compare well. Residual amplitudes are low and mostly noise. Impedance and Poisson's ratio results in Figure 10 have a reasonable range of values although Poisson's ratio is too low to the left of the well.

Conclusions

Elliptical velocity inversion results are compatible with fault and fracture description from other methods and data sets. The inversion for *P* and *S* impedance and derivative attributes produced volumes that relate to rock properties, such as brittleness and rigidity that are likely to impact fracturing.

Given the noise level in the data and the concern with regard to variability of near and far amplitudes, the prestack simultaneous inversion residual amplitudes are acceptably low. Extracted seismic *P* impedance traces are a good match to the upscaled log data; seismic *S* impedance less so, as might be expected given the data quality concerns, and the resulting Poisson's ratio, while moving in the correct sense, is lower than that of the well log. Nevertheless, geologically sensible integrated interpretation results show that this data set may be reliably used to infer information on fracture orientation and brittle/ductile layers that are important indicators of TOC and for horizontal well placement.

This project is funded by China National Natural Science Fund Grants U1262206.

References Cited

Thomsen, L., 1986, Weak elastic anisotropy: Geophysics, v. 51/10, p. 1954-1966.

Thomsen, L., 1988, Reflection seismology over azimuthally anisotropic media: Geophysics, v. 53/3, p. 304-313.

Thomsen, L., 1995, Elastic anisotropy due to aligned cracks in porous rock: Geophysical Prospecting, v. 43, p. 805-830.

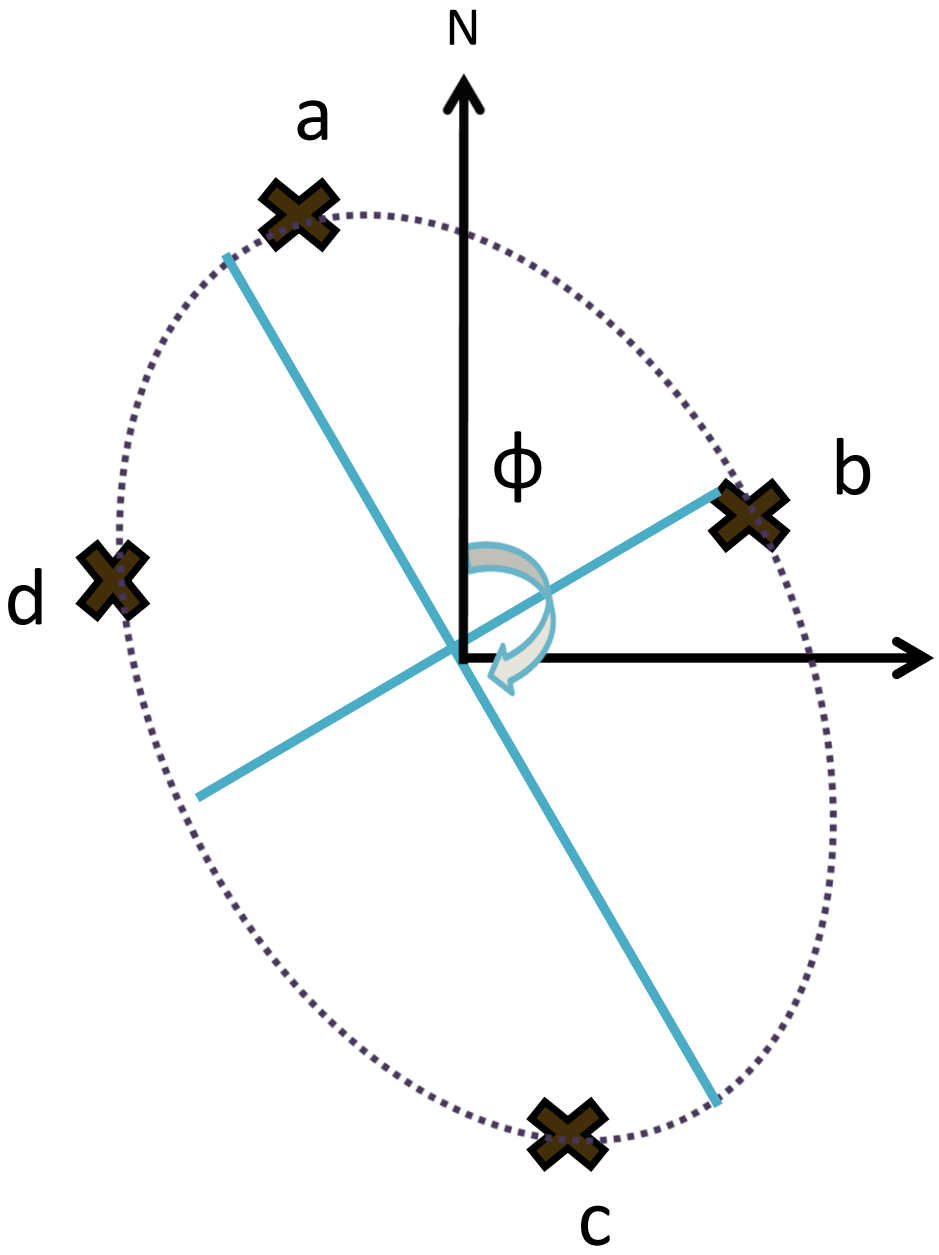

Figure 1. a–d location of sector velocities, Φ – azimuth of anisotropy plane, major axis V_{Pfast}, and minor axis V_{Pslow}.

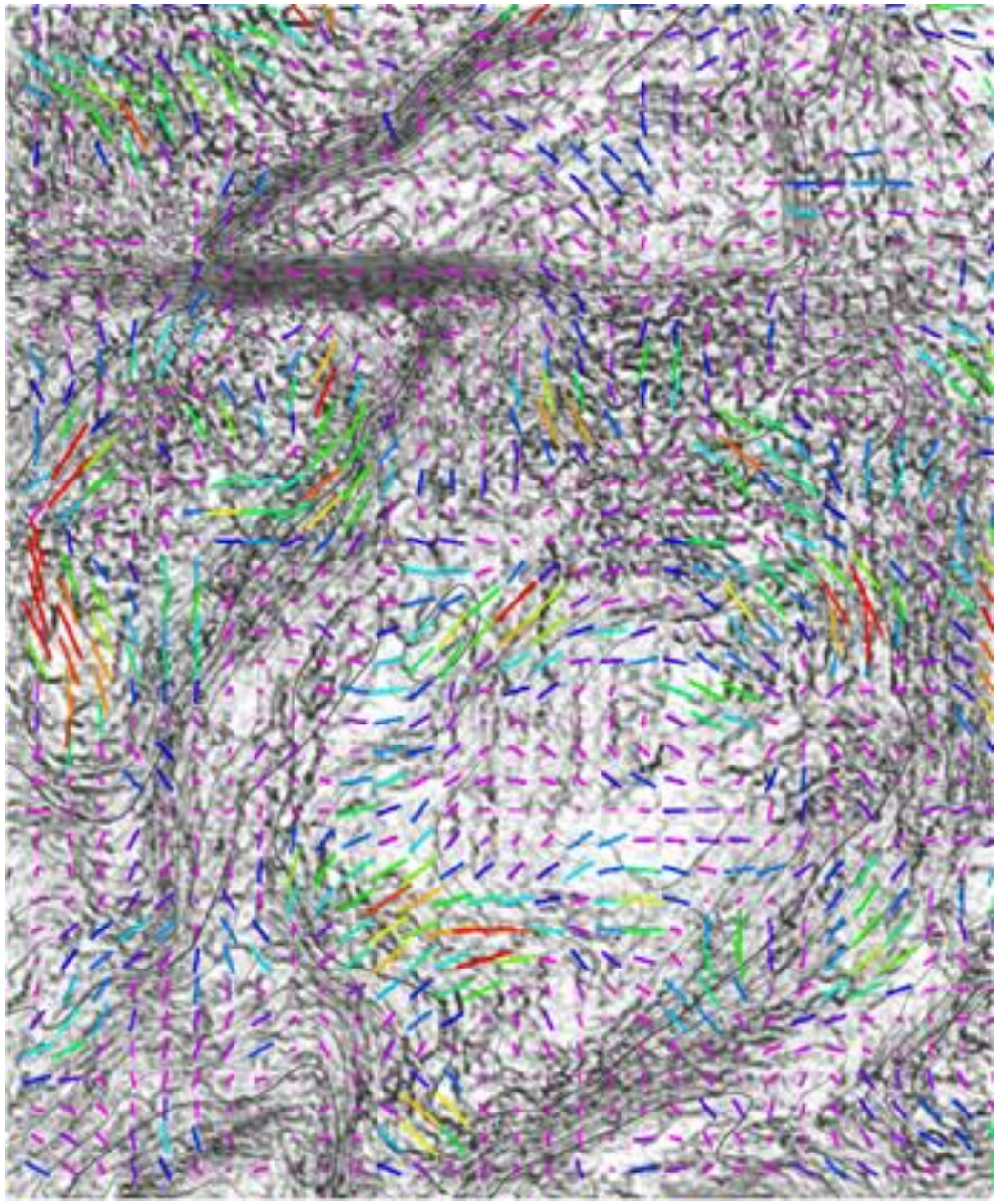

Figure 2. Coherence and anisotropy. Length and color of vectors indicate magnitude of anisotropy with vector azimuth corresponding to the azimuth of anisotropy. Analysis window is from TS – 62 ms to TS – 102 ms.

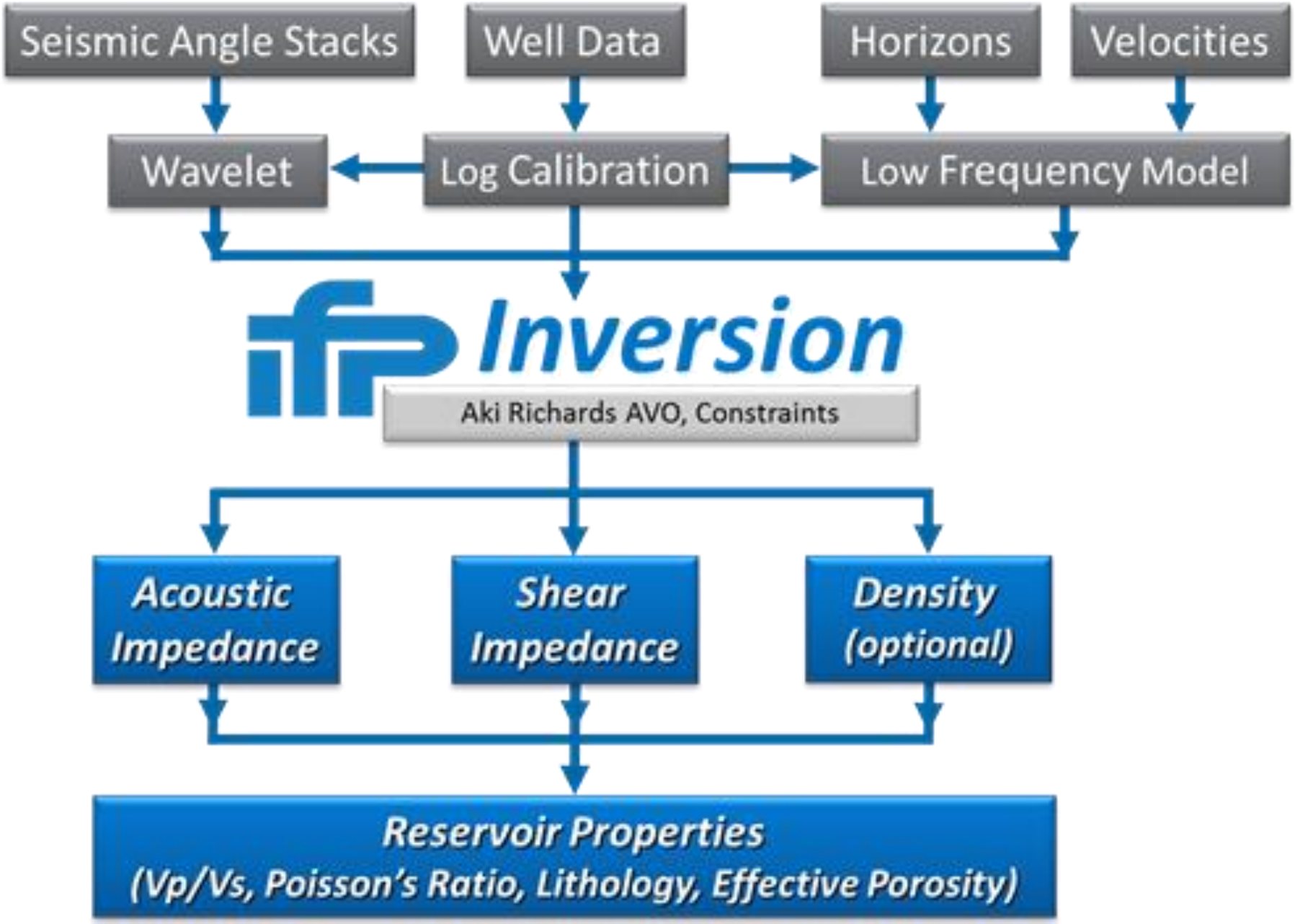

Figure 3. Simultaneous impedance inversion workflow.

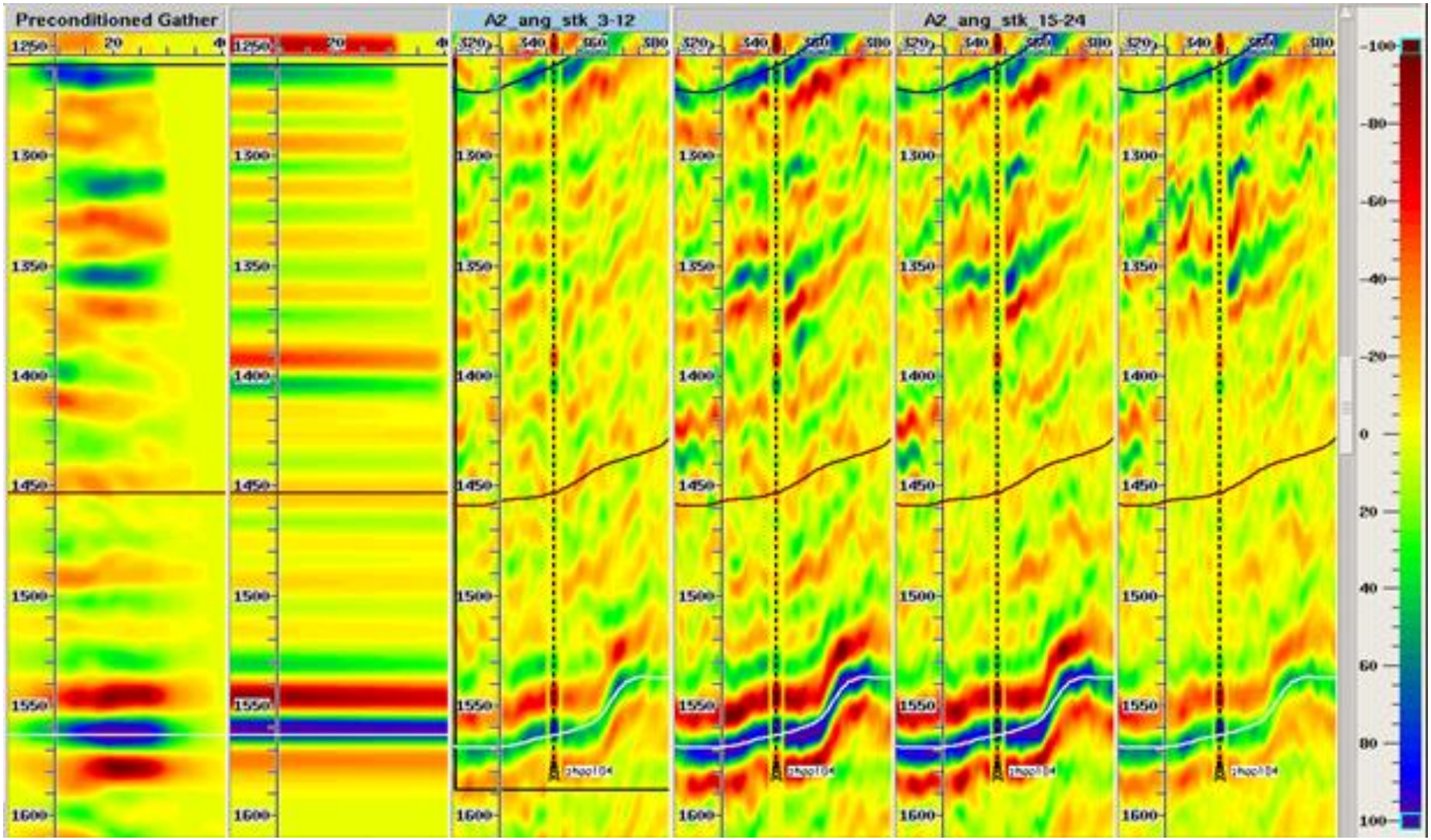

Figure 4. Synthetic to seismic tie for sector 2. Panels from left to right are conditioned seismic gather, synthetic gather, angle stacks 3-23, 9-18, 15-24, and 21-31 degrees. The synthetic angle stack is inserted in the seismic angle stack at the well location.

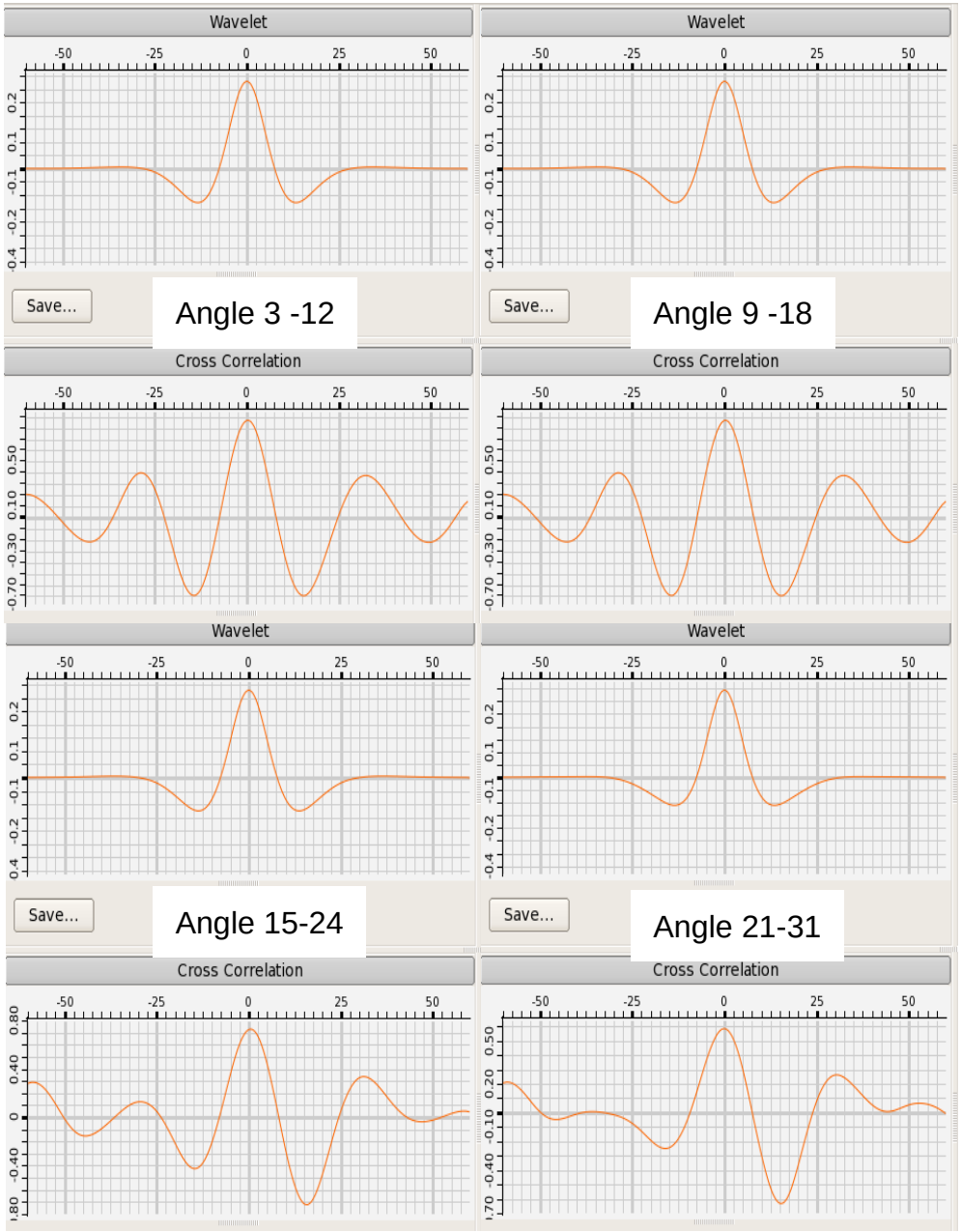

Figure 5. Extracted wavelets and cross correlation between synthetic and seismic for Sector 3 angle stacks. Cross correlation coefficients are 0.87, 0.78, 0.73, and 0.58 from near to far angles.

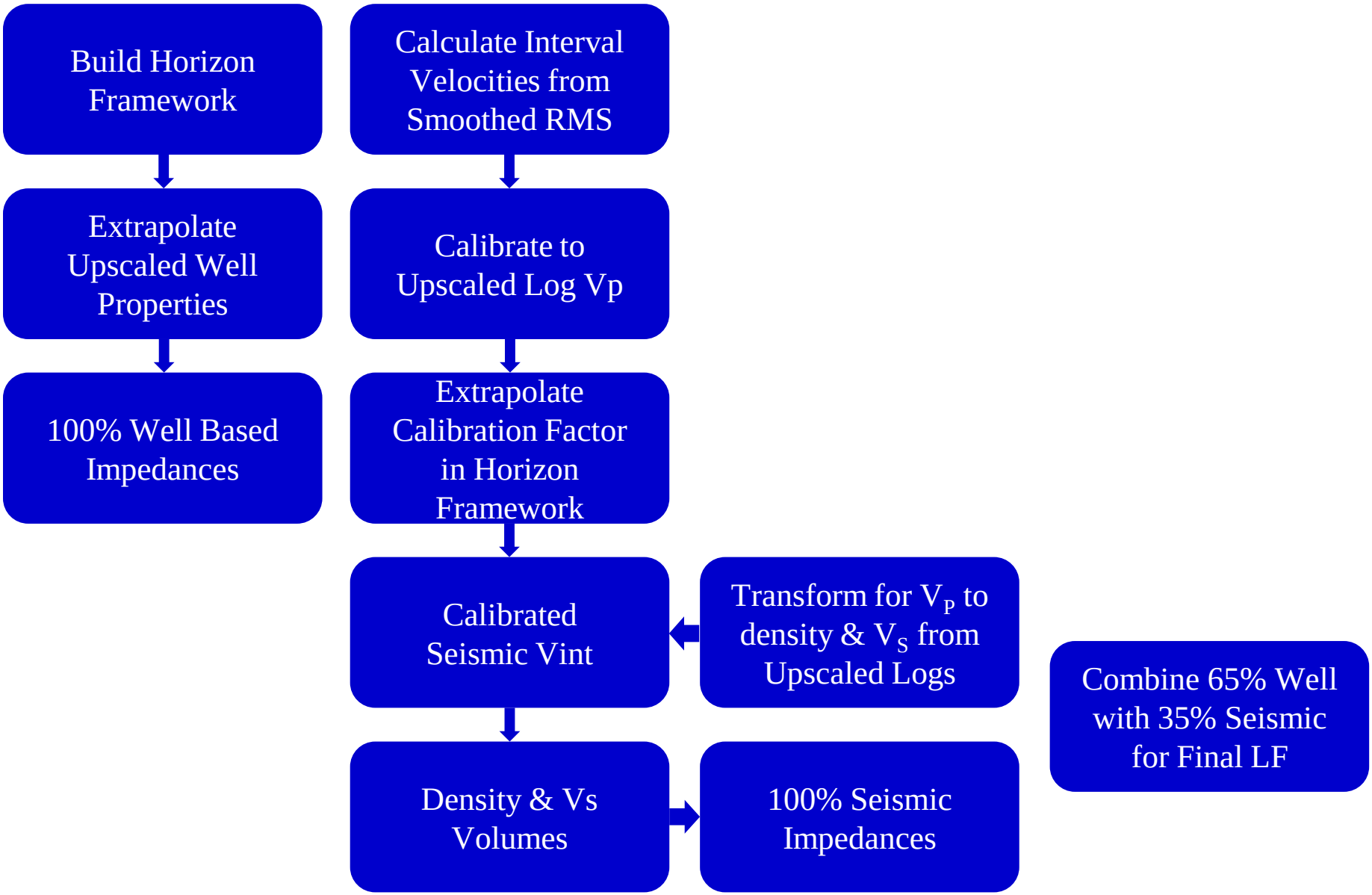

Figure 6. Low frequency volume workflow to calibrate seismic velocities to log velocities and combine seismic derived with well derived results.

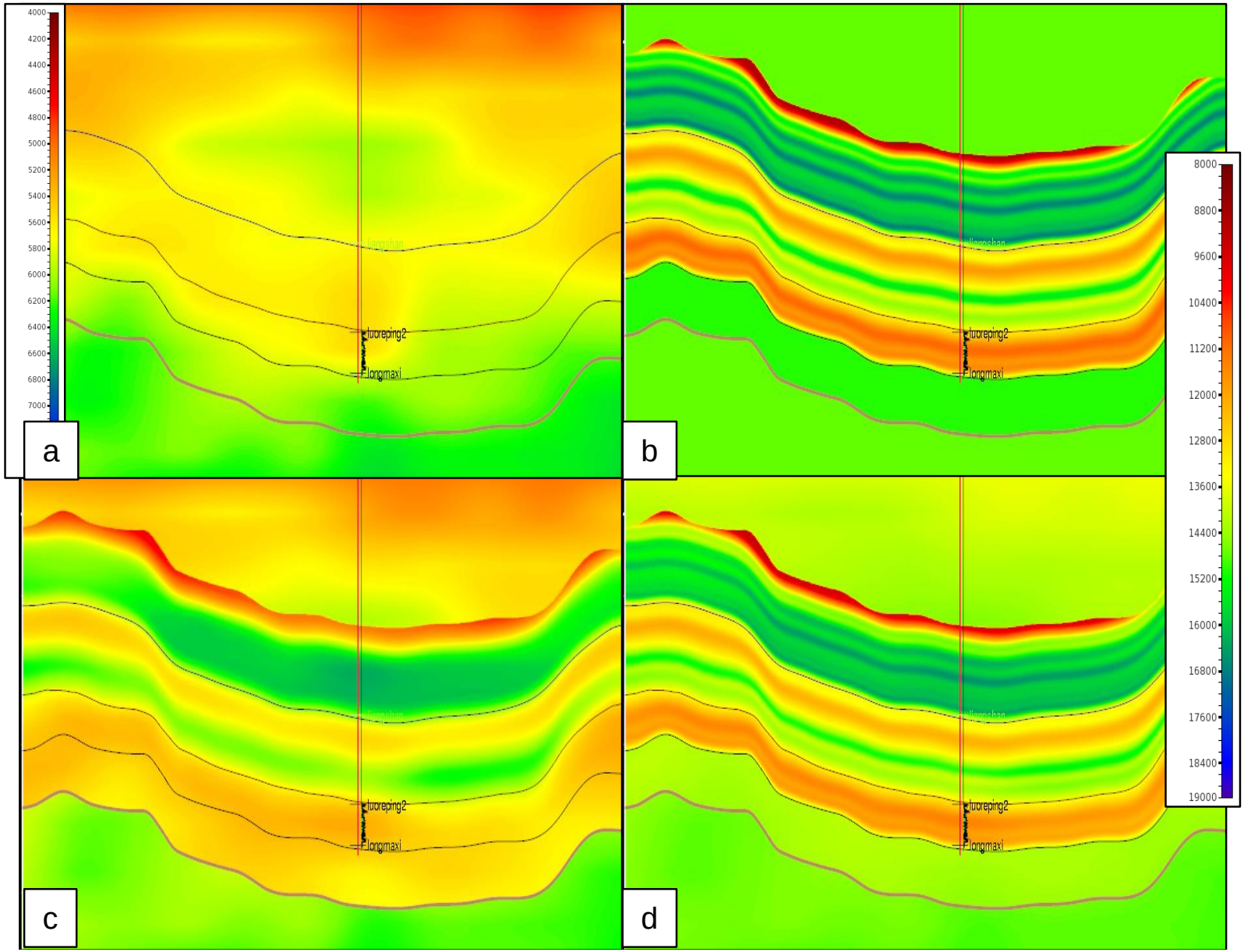

Figure 7. a, interval velocity from smoothed seismic RMS; b, P Impedance well only; c, P Impedance from seismic velocities calibrated to well; d, P Impedance 65% wells 35% seismic. The TS horizon, close to TD of well has been copied and time shifted to bound inversion window.

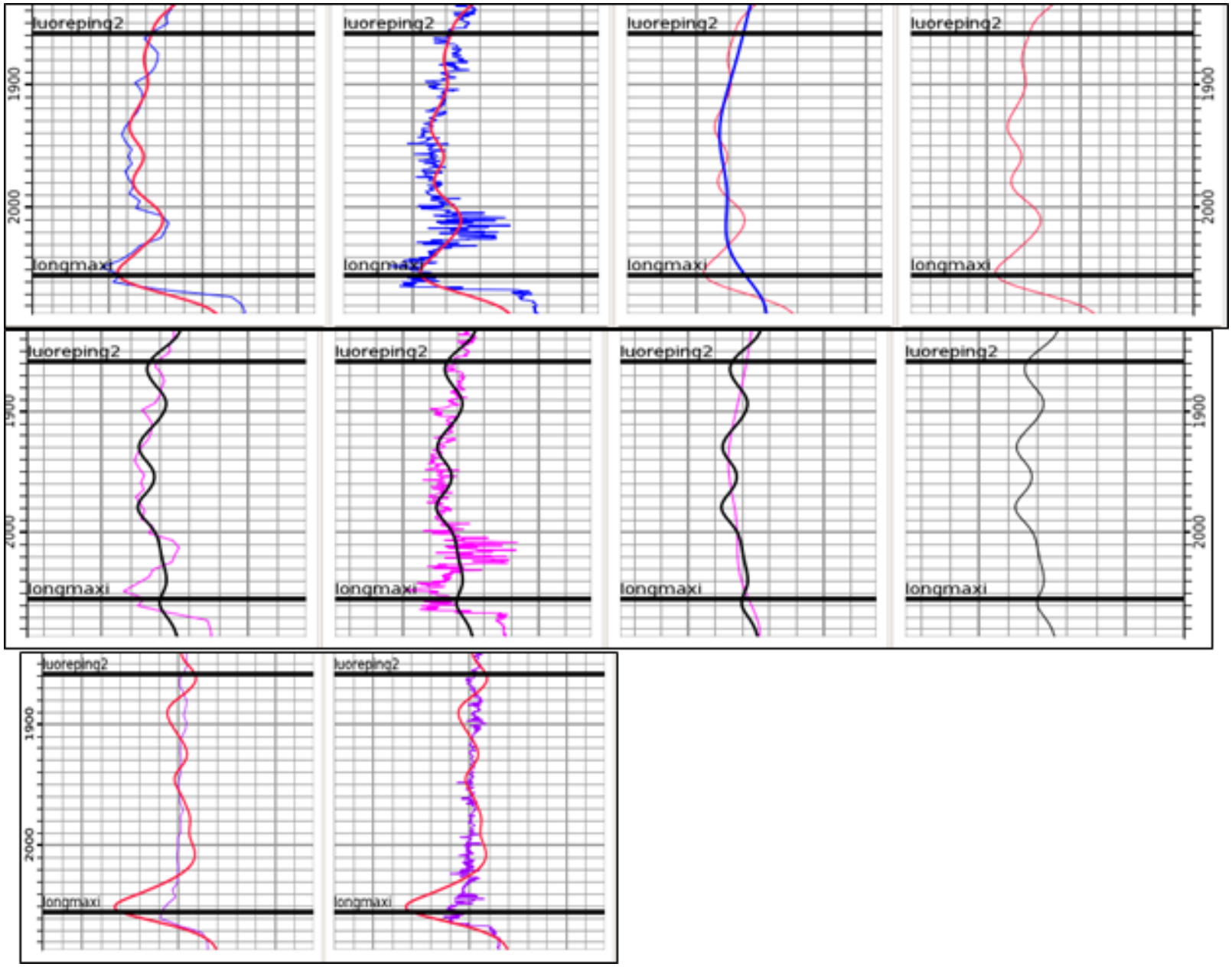

Figure 8. Top row P impedance; middle S impedance; lower Poisson's ratio. Column 1 extracted seismic (red and black) on upscaled log. Column 2 extracted seismic on log scale. Column 3 extracted seismic on low frequency trend. Column 4 extracted from seismic.

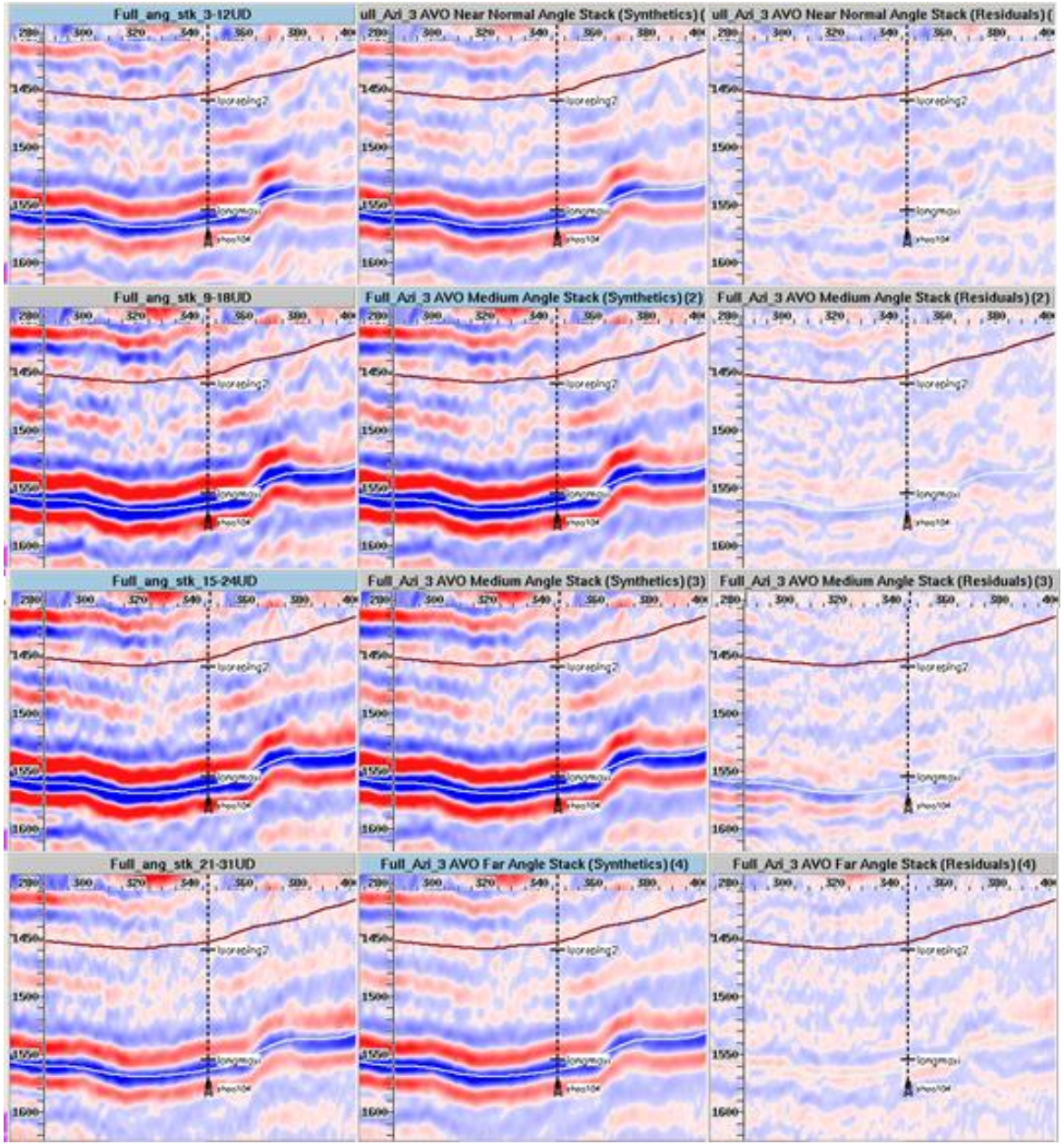

Figure 9. Angle stacks, synthetics, and residuals for full azimuth inversion. From the top row, angle stacks are 3-12 ^{o}, 9-18 ^{o}, 15-24 ^{o}, and 21-31^{o}.

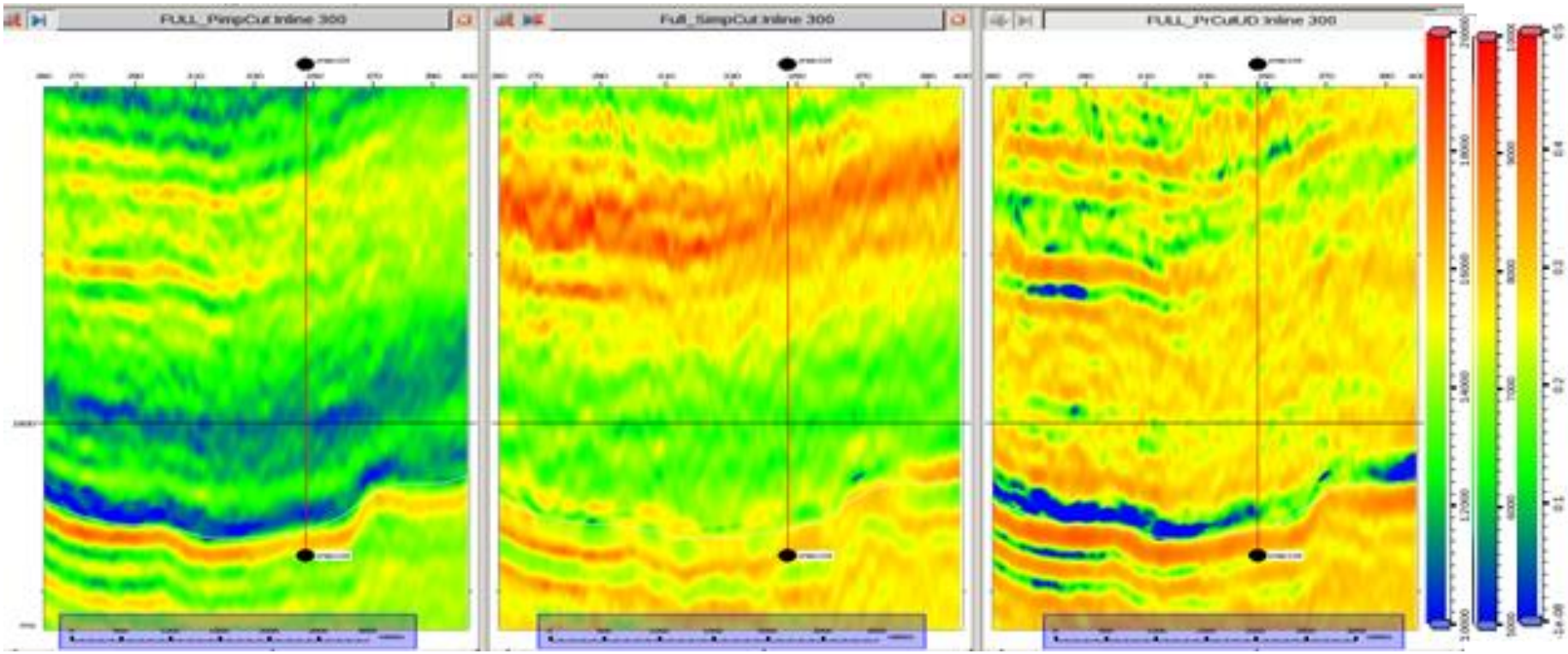

Figure 10. P impedance, S Impedance, and Poisson's ratio from full azimuth inversion.